PAPER

Covalent functionalization based heteroatom doped graphene nanosheet as a metal-free electrocatalyst for oxygen reduction reaction†

Minju Park, Taemin Lee and Byeong-Su Kim*

Oxygen reduction reaction (ORR) is an important reaction in energy conversion systems such as fuel cells and metal–air batteries. Carbon nanomaterials doped with heteroatoms are highly attractive materials for use as electrocatalysts by virtue of their excellent electrocatalytic activity, high conductivity, and large surface area. This study reports the synthesis of highly efficient electrocatalysts based on heteroatom-doped graphene nanosheets prepared through covalent functionalization using various small organic molecules and a subsequent thermal treatment. A series of nitrogen-doped reduced graphene oxide (NRGO*n*) nanosheets exhibited varying degrees and configurations of nitrogen atoms within the graphitic framework depending on the type of precursors used. On the basis of the rotating disk electrode (RDE) and rotating ring–disk electrode (RRDE) experiments, NRGO3, with a high degree of pyridinic-N content, displayed the desired one-step, quasi-four-electron transfer pathway during ORR, similar to commercial Pt/C. We also demonstrated the potential of covalent functionalization of sulfur and boron-doped graphene nanosheets.

Introduction

Increasing energy demands associated with the limited availability of fossil fuels have stimulated intense research on energy conversion and storage systems.[1] Among the many choices of energy storage systems, fuel cells and metal–air batteries have received considerable attention owing to their remarkable theoretical energy density and environmental benignity.[2–6] Despite their promising features and significant progresses, it is still desirable to develop highly efficient and cost-effective electrocatalysts for a key reaction in fuel cells and metal–air batteries, the oxygen reduction reaction (ORR). As a consequence, ORR catalysts play a pivotal role in converting oxygen as an energy source and thus determining electrochemical performance of the devices.[4,7] Traditionally, platinum and its alloys have been employed as ORR catalysts by virtue of their excellent catalytic efficiency, relatively low overpotential, and high current density.[8–10] However, they still suffer from multiple limiting factors, including intermediate tolerance, anode crossover, sluggish kinetics, and poor stability. Together with their high cost and limited reserves, they have limited use in large-scale applications.[11–15] Therefore, recent efforts have been geared toward the development of alternative catalysts based on non-precious metals and metal-free carbon-based nanomaterials. Among them, graphene, a single layer of two-dimensional aromatic carbon lattice, exhibits outstanding electrical, chemical, and mechanical properties, which are favorable in the harsh ORR environment.[16–18]

Furthermore, heteroatom-doped graphene nanosheets introduced with other heteroatoms such as nitrogen, sulfur, boron, and phosphorus have been demonstrated to exhibit excellent electrocatalytic performance toward ORR.[19–23] This heteroatom doping not only enhances the electrical properties of graphene, but also effectively affords the active site of the catalyst with a charge polarization effect.[24] In general, nitrogen-doped (N-doped) graphene is commonly prepared by several methods, including chemical vapor deposition and subsequent thermal annealing in the presence of ammonia, pyrolysis of nitrogen-containing precursors such as small molecules (melamine, pyridine), or polymers, and nitrogen-plasma treatments of graphene.[14,25–31] Although these approaches successfully introduce nitrogen atoms within the graphene framework, many of these approaches require toxic gas precursors, are limited to doping of nitrogen atoms only, or are unable to control the degree of doping and type of nitrogen functionality.

Herein, we report a unique design and characterization of new heteroatom-doped graphene nanosheets prepared through the covalent functionalization of various small organic molecules with a subsequent thermal treatment. The covalent functionalization chemistry is based on the *N*-ethyl-*N′*-(3-

Interdisciplinary School of Green Energy and School of NanoBioscience and Chemical Engineering, Ulsan National Institute of Science and Technology (UNIST), Ulsan 689-798, Korea. E-mail: bskim19@unist.ac.kr; Fax: +82-52-217-2019; Tel: +82-52-217-2923

† Electronic supplementary information (ESI) available: UV-vis spectra of all NGO*n*, tables of atomic composition and nitrogen configurations from high-resolution XPS, RDE, and stability data are provided. See DOI: 10.1039/c3nr03581f
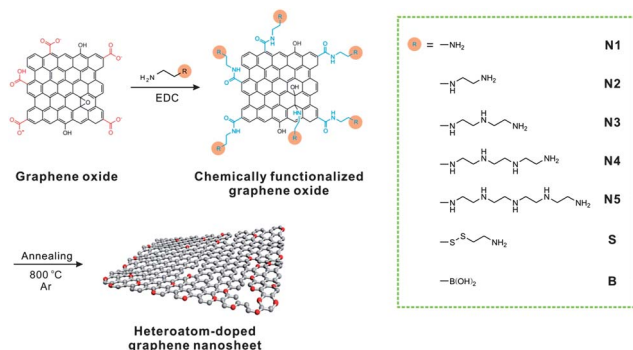
Fig. 1 Schematic representation of the surface functionalization of graphene nanosheets with various molecules.
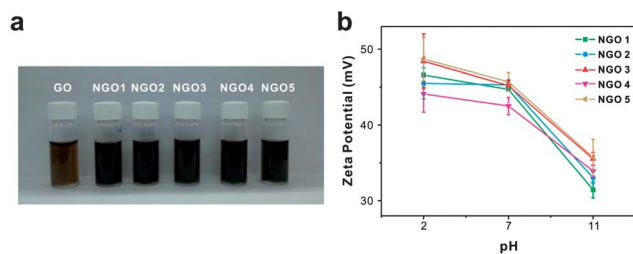

Fig. 2 (a) Photographs of each suspension prepared in this study (conc. 0.50 mg mL^{-1}). (b) Zeta-potential for functionalized NGO*n* derivatives as a function of pH.

dimethyl aminopropyl) carbodiimide methiodide (EDC)-mediated reaction between the carboxylic acid groups of graphene oxide (GO) nanosheets and the excess amine moiety in the small molecules.[32,33] The prepared heteroatom-doped graphene nanosheets exhibited good electrocatalytic activity through an efficient one-step, four-electron pathway similar to commercial Pt/C catalysts toward ORR compared to their undoped counterparts; this could be attributed to the charge polarization of the carbon network induced by heteroatoms. As a proof of concept, we employed five different types of amines with differing amine densities for the preparation of N-doped reduced graphene oxide (NGO*n*, *n* = number of amine groups) nanosheets (Fig. 1). We demonstrate how the electrochemical performance can be improved by varying the degree and configurations of the nitrogen dopant. Moreover, we successfully extended the approach toward the introduction of other heteroatoms such as boron and sulfur into the graphene nanosheet.

Results and discussion

The GO suspension was initially prepared according to the modified Hummers method starting from a commercially available graphite powder.[34] Following sonication for exfoliation of graphite oxide, the chemical functional groups introduced on the surface of the graphene nanosheet, such as carboxylic acids and alcohol groups, rendered the prepared GO suspension negatively charged over a wide range of pH

conditions (ζ-potential of −40 mV). As a model system, we used five different amine molecules as follows: ethylene diamine, diethylene triamine, triethylene tetramine, tetraethylene pentamine, and pentaethylene hexamine (Fig. 1). In order to introduce these various amine molecules, we employed the N-ethyl-N′-(3-dimethyl aminopropyl)carbodiimide methiodide (EDC)-mediated surface functionalization of graphene nanosheets through the reaction between carboxylic acids and excess amine molecules. It should be noted that we could not prevent the direct ring opening reaction of epoxides, which were present on the basal plane of GO nanosheets, with excess amine groups; nonetheless, this functionalization route also contributed to the successful introduction of amine moieties on the GO nanosheet.[32,33]

The successful functionalization of various amine molecules afforded a series of positively charged GO with varying numbers of amine groups (NGO1–NGO5) that exhibited fairly good colloidal stability for several months without any aggregations. For example, zeta-potential measurements clearly demonstrated the successful surface functionalization of GO, whose surface charge reversed from negative (−40 mV at neutral conditions) to positive upon functionalization with amine moieties that ranged from 41.7 to 52.0 mV at pH 2, 41.4 to 47.0 mV at pH 7, and 30.4 to 38.1 mV at pH 11 from NGO1 to NGO5. It is interesting to observe that the zeta-potential values of all samples decreased with an increase of pH, further supporting the presence of weakly charged amine moieties whose charge densities are highly dependent on the external pH conditions. Moreover, we noticed that the color of the GO suspension changed to a dark brown after functionalizing with amine moieties.[35,36]

Atomic force microscopy (AFM) images in Fig. 3 demonstrated that the prepared GO nanosheets were mainly comprised of a monolayer of graphene nanosheets having an average thickness of 0.90 ± 0.03 nm and a lateral dimension of 1.01 ± 0.19 μm. As a representative example, NGO3 showed that the graphene nanosheets possessed a higher average thickness of 1.26 ± 0.04 nm without noticeable changes in the lateral dimension of graphene nanosheets of 1.01 ± 0.46 μm.[37,38] This
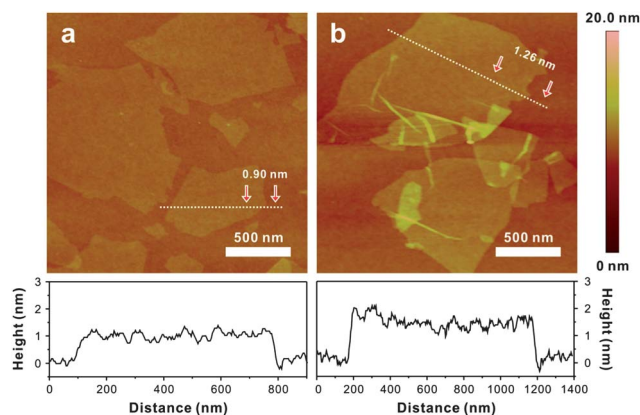

Fig. 3 Representative height-mode AFM images of (a) GO and (b) NGO3 with the corresponding line scan profiles.

observation reflects the presence of long-chain triethylene tetramine on both sides of the GO nanosheets after functionalization. In addition, it highlights the mild nature of this synthetic approach that does not alter the intrinsic properties related to the dimensions of the graphene nanosheet.

The prepared NGO*n* catalysts were subjected to thermal annealing at 800 °C for 1 h under an Ar atmosphere. The resulting products were denoted as N-doped reduced GO nanosheets (NRGO*n*) according to the respective amine precursors. We propose here that the degree of nitrogen content in the molecules affects the degree of nitrogen content and its configuration in the NRGO*n*. The thermal annealing approach caused atomic rearrangement leading to a highly ordered graphitic structure and the simultaneous incorporation of nitrogen atoms from the functionalized amine groups into the graphene matrix.[39] The successful incorporation and the nature of N-doping on the graphene nanosheets were identified by X-ray photoelectron spectroscopy (XPS) (Fig. 4). From the XPS survey spectra, we found a distinct evolution of nitrogen peak in all NRGO*n* samples, which was absent in the GO nanosheets annealed under identical conditions (*i.e.* thermally reduced GO (TRGO)). The deconvoluted high-resolution N1s XPS spectra further elucidated four different types of nitrogen configurations on the graphene nanosheets, which are pyridinic-N (N-6, 398.1 eV), pyrrolic-N (N-5, 399.8 eV), graphitic-N (N-Q, 401.2 eV) and N-oxide (N–O, 403.1 eV) from NRGO*n*. In accordance with the nitrogen content in the initial amine molecules, the amount of doped nitrogen was gradually increased from NRGO1 (0.72%) to NRGO5 (4.3%). It is worth mentioning that the relative fractions of N-configurations were different depending on the amine precursors used (Table S1†). In general, it has been known that pyridinic-N is the most efficient bonding structure to improve ORR activity in graphene. In our study, NRGO3 has the most abundant pyridinic-N functionality despite its relatively lower N-content.
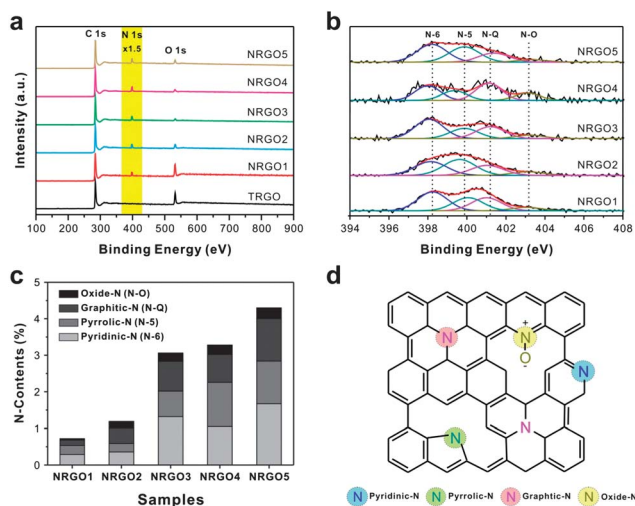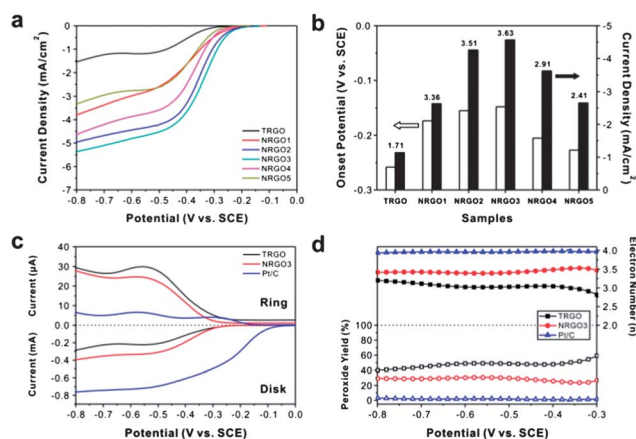

Fig. 5 (a) Linear sweep voltammograms (LSVs) of all NRGO*n* electrocatalysts prepared in the study, including that of a control set of TRGO. RDE tests were acquired at a rotation rate of 2500 rpm and a scan rate of 10 mV s⁻¹ in O₂-saturated 0.10 M KOH electrolyte solution. (b) Comparison of the onset potential (white bar) and limiting current density (black bar) of each catalyst as determined by RDE experiments. The electron transfer number (*n*) based on the Koutecky–Levich equation is located on the top of the bar graph. The onset potential and limiting current were measured at −0.02 mA cm⁻² and −0.50 V (*vs.* SCE), respectively. (c) LSVs of RRDE experiments of TRGO, NRGO3, and commercial 20 wt% Pt/C catalysts in an O₂-saturated 0.10 M KOH aqueous solution at 3200 rpm. (d) The plot of the peroxide yields (%) and the electron transfer number (*n*) of electrocatalysts.

To explore the electrocatalytic activity during the ORR process of NRGO*n* catalysts, we recorded the rotating disk electrode (RDE) voltammograms in an O₂-saturated 0.10 M KOH aqueous solution (Fig. 5 and S3†). As a control experiment, undoped TRGO was employed to verify the effect of N-doping for an efficient ORR. Fig. 5 shows a series of polarization curves at a constant rotating rate of 2500 rpm and quantitative evaluation in terms of the onset potential and kinetic limiting current density based on the RDE measurements. The electron transfer number (*n*) of each catalyst was also calculated during the ORR process from the RDE results based on the Koutecky–Levich (K–L) equation.[40,41] All NRGO*n* catalysts displayed considerably enhanced electrocatalytic activity unlike undoped TRGO, which showed a dominant two-step, two-electron ORR pathway. Among all NRGO*n* catalysts, the ORR activity of NRGO3 was found to exhibit the best catalytic performance with the most positive onset potential at −0.15 V and the highest limiting current density of −4.55 mA cm⁻². Moreover, the electron transfer number of NRGO3 determined from the K–L plot reached 3.63, suggesting an efficient four-electron ORR pathway similar to that of commercial Pt/C catalysts.[42,43] The pyridinic-N sites have been widely recognized as catalytic active sites for ORR because of the delocalization of the π-electrons from pyridinic-N.[44] XPS experiments provided additional support to the theory that highly catalytic carbon materials usually retain a large amount of pyridinic-N.[21,45] Thus, it is proposed that the enhanced catalytic activity of NRGO3 originates from the higher fraction of pyridinic-N rather than the absolute amount of N-doping of the graphene nanosheets (*i.e.*, 43.2% of NRGO3 *vs.* 32.0% of NRGO4 *vs.* 38.9% of NRGO5).

Fig. 4 (a) XPS survey spectra for various samples investigated in this study. (b) Deconvoluted high-resolution XPS N1s spectra of all NRGO*n*. (c) Total N contents of NRGO*n*. (d) Schematic representation of nitrogen bonding configurations in N-doped graphene nanosheets.
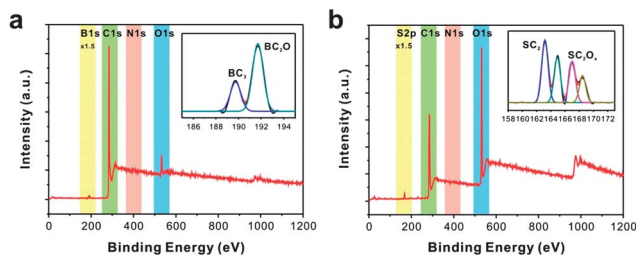
Fig. 6 XPS survey spectra of (a) B-doped and (b) S-doped graphene nanosheets with corresponding deconvoluted high-resolution B1s and S2p spectra in the inset, respectively.

To further verify the ORR activity with the optimized NRGO3 catalyst in comparison with those of undoped TRGO and commercial Pt/C catalysts, rotating ring–disk electrode (RRDE) measurements were carried out to monitor the formation of hydrogen peroxide species (HO_2^-) during the ORR process (Fig. 5c and d). The RRDE measurements showed that NRGO3 exhibited a higher disk current (oxygen reduction) and a smaller ring current (peroxide oxidation) than the undoped TRGO catalyst. The calculated electron transfer number (n) was around 3.45 and peroxide yield was around 28% from -0.3 to -0.8 V, while TRGO showed that the electron number (n) was around 3.12 and peroxide yield was about 44% at the identical potential range. This result is consistent with that obtained from the K–L plot based on the RDE measurements, suggesting that the NRGO3 catalyst can undergo a one-step, direct four-electron ORR pathway with a relatively low yield of the peroxide intermediate. Although the catalytic performance of NRGO3 is still inferior to that of commercial Pt/C, the former displayed a significantly enhanced durability. The durability test was conducted at a constant reduction potential of -0.3 V. After 10 000 s, the chronoamperometric responses of NRGO3 showed a slow attenuation with high current retention of 73%, which is a much higher value than that of commercial Pt/C with 60% (Fig. S4†). This confirmed that the metal-free NRGO electrocatalyst has a much better stability for ORR in an alkaline environment.

Finally, we extended our current approach toward other heteroatoms such as boron and sulfur.[14,46,47] As a molecular precursor of each doping atom, we employed 4-aminophenylboronic acid as a boron source and cystamine as a sulfur source. Interestingly, each heteroatom was well incorporated within the graphene matrix together with the nitrogen dopant, as we employed an identical chemical functionalization process on the graphene nanosheets. High-resolution XPS shows that each heteroatom is found to be in different configurations (Fig. 6).

Conclusion

In summary, we present a simple approach for chemical functionalization toward heteroatom-doped graphene nanosheets with small organic molecules for use as electrocatalysts for the oxygen reduction reaction. The prepared heteroatom-doped graphene nanosheet exhibited a good electrocatalytic activity

through an efficient one-step, four-electron pathway similar to that exhibited by a commercial Pt/C catalyst, compared to its undoped counterpart. This can be attributed to the charge polarization of the carbon network induced by the heteroatoms. Furthermore, nitrogen-doped graphene nanosheets showed superior stability compared to commercial Pt/C catalysts. This approach has also been successfully extended to other heteroatoms such as boron and sulfur on the graphene nanosheets. By taking advantage of the facile synthesis process, we anticipate that this covalent functionalization would afford other routes for the controlled introduction of heteroatoms on the graphene nanosheets for various applications.

Experimental section

Preparation of graphene oxide (GO) suspension and covalent surface modification

Initially, graphite oxide powder was prepared from graphite powder (Aldrich, <20 mm) by the modified Hummers method and exfoliated to give a brown dispersion of graphene oxide (GO) under ultrasonication (typical conc. of 0.50 mg mL^{-1}). For the surface functionalization, 50 mL of the GO suspension was reacted with 4 mL of various amines (ethylene diamine, diethylene triamine, triethylene tetramine, tetraethylene pentamine, and pentaethylene hexamine) in the presence of 0.50 g of N-ethyl-N'-(3-dimethyl aminopropyl)carbodiimide methiodide (EDC) for 12 h at room temperature, followed by an extensive dialysis (SpectraPore MWCO 12–14k) for 3 days to remove any byproducts and excess reactants. These suspensions were denoted as amine-functionalized graphene oxide (NGOn).

Preparation of nitrogen-doped reduced graphene oxide (NRGO) and thermally reduced graphene oxide (TRGO)

The NGOn suspensions were freeze dried to remove water and annealed at 800 °C for 1 h under an Ar atmosphere to afford nitrogen-doped graphene oxide (NRGOn) powder. Thermally reduced graphene oxide (TRGO) was prepared by annealing GO powder under identical conditions.

Preparation of catalyst ink for the rotating disk electrode

Each NRGOn powder was first dispersed in a solvent mixture (water : Nafion = 9 : 1 v/v) at a concentration of 1.0 mg mL^{-1} with a brief sonication for 40 min to obtain homogeneous dispersions. Then 5 µL of each suspension was dropped on a 3 mm diameter glassy carbon electrode embedded in Teflon as a working electrode. Finally, ink was dried under vacuum conditions for 10 min forming a thin film on the glassy carbon electrode.

Rotating disk electrode (RDE) experiment

For the electrocatalytic evaluation of NRGOn, we performed the rotating disk electrode (RDE) experiment at room temperature by linear sweep voltammograms (LSVs). An as-prepared glassy carbon electrode was used as a working electrode, Pt was used as a counter electrode and saturated calomel electrode (SCE) was used as a reference electrode. RDE measurements were

carried out in a 0.1 M KOH electrolyte in the potential range from 0 V to −0.8 V at a scan rate of 10 mV s^{-1} and measured at 900, 1600, 2500, and 3200 rpm. Oxygen was purged into the electrolyte to make an O_2-saturated solution. The Koutecky–Levich (K–L) equation was used to calculate the number of electrons transferred with RDE data.

Rotating ring–disk electrode (RRDE) experiment

The RRDE experiments were measured at a 10 mV s^{-1} scan rate from 0 V to −0.8 V and the oxidation potential of the ring–disk was set to 0.2 V. Electron transfer number (n) and peroxide yield (%) was calculated by the following equations:

$$HO_2^{-}(\%) = 200 \frac{(I_r/N)}{I_d + (I_r/N)} \tag{1}$$

$$n = 4 \frac{I_d}{I_d + (I_r/N)} \tag{2}$$

where I_r and I_d are the ring current and the disk current, respectively.

Characterizations

UV/vis spectra were recorded using a Shimadzu UV-1800 spectrometer and the ζ-potential of colloidal suspensions was measured using a zeta potential analyzer (Malvern, Zetasizer nano-zs). The surface morphology of GO and NGO was examined using an atomic force microscope (AFM, Dimension D3100, Veeco), and we used a silicon wafer as a substrate to obtain the AFM image of NGO3 graphene nanosheets before thermal annealing. X-ray photoelectron spectroscopy (XPS, Thermo Fisher, K-alpha) was used to detect elemental composition and the chemical state of the NRGO suspensions. Electrochemical performance for ORR was determined using the rotating disk electrode (RDE) and rotating ring–disk electrode (RRDE; ALS Co., Ltd).

Acknowledgements

Notes and references

1 A. S. Arico, P. Bruce, B. Scrosati, J.-M. Tarascon and W. van Schalkwijk, *Nat. Mater.*, 2005, **4**, 366.

2 J. M. Tarascon and M. Armand, *Nature*, 2001, **414**, 359.

3 G. Girishkumar, B. McCloskey, A. C. Luntz, S. Swanson and W. Wilcke, *J. Phys. Chem. Lett.*, 2010, **1**, 2193.

4 B. C. H. Steele and A. Heinzel, *Nature*, 2001, **414**, 345.

5 S. Park, J. M. Vohs and R. J. Gorte, *Nature*, 2000, **404**, 265.

6 M. Winter and R. J. Brodd, *Chem. Rev.*, 2004, **104**, 4245.

7 H. B. Heersche, P. Jarillo-Herrero, J. B. Oostinga, L. M. K. Vandersypen and A. F. Morpurgo, *Nature*, 2007, **446**, 56.

8 T. Toda, H. Igarashi, H. Uchida and M. Watanabe, *J. Electrochem. Soc.*, 1999, **146**, 3750.

9 U. A. Paulus, A. Wokaun, G. G. Scherer, T. J. Schmidt, V. Stamenkovic, N. M. Markovic and P. N. Ross, *Electrochim. Acta*, 2002, **47**, 3787.

10 V. R. Stamenkovic, B. Fowler, B. S. Mun, G. Wang, P. N. Ross, C. A. Lucas and N. M. Marković, *Science*, 2007, **315**, 493.

11 X. Yu and S. Ye, *J. Power Sources*, 2007, **172**, 145.

12 Z. Peng and H. Yang, *J. Am. Chem. Soc.*, 2009, **131**, 7542.

13 F. A. de Bruijn, V. A. T. Dam and G. J. M. Janssen, *Fuel Cells*, 2008, **8**, 3.

14 L. Lai, J. R. Potts, D. Zhan, L. Wang, C. K. Poh, C. Tang, H. Gong, Z. Shen, J. Lin and R. S. Ruoff, *Energy Environ. Sci.*, 2012, **5**, 7936.

15 Z. Jin, H. Nie, Z. Yang, J. Zhang, Z. Liu, X. Xu and S. Huang, *Nanoscale*, 2012, **4**, 6455.

16 A. K. Geim and K. S. Novoselov, *Nat. Mater.*, 2007, **6**, 183.

17 K. S. Novoselov, A. K. Geim, S. V. Morozov, D. Jiang, M. I. Katsnelson, I. V. Grigorieva, S. V. Dubonos and A. A. Firsov, *Nature*, 2005, **438**, 197.

18 A. H. Castro Neto, F. Guinea, N. M. R. Peres, K. S. Novoselov and A. K. Geim, *Rev. Mod. Phys.*, 2009, **81**, 109.

19 L. Qu, Y. Liu, J.-B. Baek and L. Dai, *ACS Nano*, 2010, **4**, 1321.

20 D. Yu, L. Wei, W. Jiang, H. Wang, B. Sun, Q. Zhang, K. Goh, R. Si and Y. Chen, *Nanoscale*, 2013, **5**, 3457.

21 S. Yang, X. Feng, X. Wang and K. Müllen, *Angew. Chem., Int. Ed.*, 2011, **50**, 5339.

22 S. Yang, L. Zhi, K. Tang, X. Feng, J. Maier and K. Müllen, *Adv. Funct. Mater.*, 2012, **22**, 3634.

23 Z.-W. Liu, F. Peng, H.-J. Wang, H. Yu, W.-X. Zheng and J. Yang, *Angew. Chem., Int. Ed.*, 2011, **50**, 3257.

24 L. Zhang and Z. Xia, *J. Phys. Chem. C*, 2011, **115**, 11170.

25 D. Wei, Y. Liu, Y. Wang, H. Zhang, L. Huang and G. Yu, *Nano Lett.*, 2009, **9**, 1752.

26 X. Wang, X. Li, L. Zhang, Y. Yoon, P. K. Weber, H. Wang, J. Guo and H. Dai, *Science*, 2009, **324**, 768.

27 Z.-H. Sheng, L. Shao, J.-J. Chen, W.-J. Bao, F.-B. Wang and X.-H. Xia, *ACS Nano*, 2011, **5**, 4350.

28 Y. Wang, Y. Shao, D. W. Matson, J. Li and Y. Lin, *ACS Nano*, 2010, **4**, 1790.

29 Z. Yan, Z. Peng, Z. Sun, J. Yao, Y. Zhu, Z. Liu, P. M. Ajayan and J. M. Tour, *ACS Nano*, 2011, **5**, 8187.

30 X. Li, H. Wang, J. T. Robinson, H. Sanchez, G. Diankov and H. Dai, *J. Am. Chem. Soc.*, 2009, **131**, 15939.

31 Y.-C. Lin, C.-Y. Lin and P.-W. Chiu, *Appl. Phys. Lett.*, 2010, **96**, 133110.

32 H. Hwang, P. Joo, M. S. Kang, G. Ahn, J. T. Han, B.-S. Kim and J. H. Cho, *ACS Nano*, 2012, **6**, 2432.

33 D. W. Lee, T.-K. Hong, D. Kang, J. Lee, M. Heo, J. Y. Kim, B.-S. Kim and H. S. Shin, *J. Mater. Chem.*, 2011, **21**, 3438.

34 W. S. Hummers and R. E. Offeman, *J. Am. Chem. Soc.*, 1958, **80**, 1339.

35 S. Stankovich, D. A. Dikin, R. D. Piner, K. A. Kohlhaas, A. Kleinhammes, Y. Jia, Y. Wu, S. T. Nguyen and R. S. Ruoff, *Carbon*, 2007, **45**, 1558.

36 S. Stankovich, R. D. Piner, X. Chen, N. Wu, S. T. Nguyen and R. S. Ruoff, *J. Mater. Chem.*, 2006, **16**, 155.

37 G. Eda, G. Fanchini and M. Chhowalla, *Nat. Nanotechnol.*, 2008, **3**, 270.

38 X. Zhou, X. Huang, X. Qi, S. Wu, C. Xue, F. Y. C. Boey, Q. Yan, P. Chen and H. Zhang, *J. Phys. Chem. C*, 2009, **113**, 10842.

39 M. Zhong, E. K. Kim, J. P. McGann, S.-E. Chun, J. F. Whitacre, M. Jaroniec, K. Matyjaszewski and T. Kowalewski, *J. Am. Chem. Soc.*, 2012, **134**, 14846.

40 J. Koutecký and V. Levich, *Zh. Fiz. Khim.*, 1958, **32**, 1565.

41 C. Hu, Y. Xiao, Y. Zhao, N. Chen, Z. Zhang, M. Cao and L. Qu, *Nanoscale*, 2013, **5**, 2726.

42 K. Lee, L. Zhang, H. Lui, R. Hui, Z. Shi and J. Zhang, *Electrochim. Acta*, 2009, **54**, 4704.

43 D. Geng, Y. Chen, Y. Chen, Y. Li, R. Li, X. Sun, S. Ye and S. Knights, *Energy Environ. Sci.*, 2011, **4**, 760.

44 C. V. Rao, C. R. Cabrera and Y. Ishikawa, *J. Phys. Chem. Lett.*, 2010, **1**, 2622.

45 K. R. Lee, K. U. Lee, J. W. Lee, B. T. Ahn and S. I. Woo, *Electrochem. Commun.*, 2010, **12**, 1052.

46 Z. Yang, Z. Yao, G. Li, G. Fang, H. Nie, Z. Liu, X. Zhou, X. Chen and S. Huang, *ACS Nano*, 2011, **6**, 205.

47 Z.-S. Wu, W. Ren, L. Xu, F. Li and H.-M. Cheng, *ACS Nano*, 2011, **5**, 5463.